Brazilian Journal
of Chemical
Engineering

ISSN 0104-6632
Printed in Brazil
www.abeq.org.br/bjche

Vol. 33, No. 03, pp. 567 - 576, July - September, 2016
dx.doi.org/10.1590/0104-6632.20160333s20150074

CHARACTERISATION OF ASYMMETRIC ALUMINA HOLLOW FIBRES: APPLICATION FOR HYDROGEN PERMEATION IN COMPOSITE MEMBRANES

N. M. Terra, C. O. T. Lemos, F. B. da Silva, V. L Cardoso and M. H. M. Reis*

Universidade Federal de Uberlândia, Faculdade de Engenharia Química, Av. João Naves de Ávila 2121,
Zip Code: 38048100, Uberlândia - MG, Brazil.
E-mail: miria@feq.ufu.br

(Submitted: February 7, 2015 ; Revised: July 27, 2015 ; Accepted: August 6, 2015)

Abstract - Asymmetric alumina hollow fibres produced by the phase inversion/sintering method present advantages in that high area/volume ratios and low mass transfer resistances are achieved due to the geometric configuration and the pore size distribution, respectively. Here we characterise hollow fibres that were prepared with different internal coagulants and at different sintering temperatures. Additionally, a palladium membrane was deposited on these different hollow fibres and hydrogen permeabilities through them were compared. More fingers were obtained when a mixture of solvent with water was used as internal coagulant, instead of pure water. At the same sintering temperature, nitrogen permeance through the fibre was increased 5-fold when a mixture of solvent and water was used as internal coagulant instead of pure solvent, and the water flux was increased 7-fold. The decrease in the sintering temperature increased the water permeance through the fibre from 21.4 to 63.9 L h^{-1} m^{-2} kPa^{-1}, but decreased its mechanical strength from 74 to 41 MPa. The hydrogen permeance at 450 °C was increased from $5.54x10^{-5}$ to $3.06\ x10^{-3}$ mol m^{-2} s^{-1} kPa^{-1} when using a more permeable hollow fibre as substrate. These results elucidate better conditions to fabricate hollow fibres that present low mass transfer resistances.
Keywords: Asymmetric hollow fibres; Composite palladium membranes; Hydrogen permeation.

INTRODUCTION

Membrane separation processes have been widely used in different areas such as chemical, food and pharmaceutical industries. Depending on the desired application, membranes can be synthesized from different materials, in different geometries and with symmetric or asymmetric pore size distributions. Ceramic membranes in a hollow fibre configuration present some advantages due to the high chemical, thermal and mechanical resistances of the applied material, in addition to the membrane geometry that enables a large surface area per unit volume of a membrane module.

Conventionally, ceramic membranes are fabricated by the deposition of several layers in which each step includes a heat treatment. The immersion induced phase inversion method, first described by Loeb and Sourirajan (1963) for polymeric membranes, allows the development of an asymmetric membrane structure in a single step (de Jong *et al.*, 2004; Tan *et al.*, 2001; Machado *et al.*, 1999; Falbo *et al.*, 2014). A plurality of finger-like voids or microchannels within the membranes is formed due to the viscous fingering phenomenon that takes place concurrent to phase inversion. Different from the immer-

*To whom correspondence should be addressed
This is an extended version of the work presented at the 20th Brazilian Congress of Chemical Engineering, COBEQ-2014, Florianópolis, Brazil.

sion induced phase inversion technique applied in the production of polymeric membranes, the formation of ceramic asymmetric membranes occurs due to the hydrodynamically unstable viscous fingering phenomena, since a high viscous suspension is in contact with a low viscous hydrophilic nonsolvent (Wei*, et al.*, 2008). Hydrodynamically unstable viscous fingering is a well-known phenomenon that occurs at the interface between fluids with different viscosities in the first moment of mixing. For ceramic membranes, the dry-wet spinning and phase-inversion technique is followed by a sintering process.

Asymmetric membranes present at least two main regions of different pore sizes: a sponge-like layer with smaller pore sizes and a region with microchannels of larger pore sizes. The sponge-like layer ensures the necessary mechanical strength for the membrane. Thus, the asymmetric pore structure with an outer sponge layer and an inner layer with larger filaments presents favourable characteristics for higher permeations (Garcia-Garcia *et al.*, 2011).

Characteristics of asymmetric ceramic membranes are mainly influenced by process parameters such as suspension composition, air gap, extrusion rate, bore liquid flow rate and sintering temperature (Lee *et al.*, 2014; Liu *et al.*, 2003; Sun *et al.*, 2006; Kingsbury and Li, 2009; Li *et al.*, 2006). Garcia-Garcia *et al.* (2011 2012) showed that the increase in the sintering temperature increased the bending strength of the membrane but decreased its permeability. Therefore, there is a trade-off between mechanical strength and gas permeability and this choice must be deeply analysed.

Composite palladium (Pd) membranes can be applied for hydrogen purification in an integrated membrane reactor system (Yun and Oyama, 2011). However, one of the main drawbacks in this application is the increase in the hydrogen permeability (Dittmeyer *et al.*, 2001). This increase can be achieved by reducing the palladium thickness, but without loss of the membrane selectivity. Moreover, the substrate used for the palladium deposition must present low mass transfer resistance, but confer the necessary mechanical strength to the composite membrane. Asymmetric hollow fibres can be potentially applied as a substrate for palladium membrane depositions due to their smooth outer layer and low mass transfer resistance (Hatim *et al.*, 2011).

The main objective of this research was to evaluate the characteristics of alumina (Al_2O_3) hollow fibres prepared using different sintering temperatures and internal coagulant compositions. These hollow fibres were characterised according to their morphology, roughness, mechanical strength, and water and nitrogen permeabilities. Additionally, a comparison of hydrogen permeabilities through composite Pd/Al_2O_3 membranes that were prepared using different hollow fibres as supports was carried out.

MATERIAL AND METHODS

Material

Ceramic hollow fibre substrates were fabricated using aluminium oxide powder of 1.0 μm (alpha, 99.9% metal basis, surface area 6-8 $m^2\ g^{-1}$) purchased from Alfa Aesar. The ceramic suspension was prepared using Polyethersulfone (PESf, Radel A-300, Ameco Performance, USA), dimethyl sulfoxide (DMSO, VWR) and Arlacel P135 (Uniqema, UK) as polymer binder, solvent and additive, respectively.

Tin(II) chloride dihydrate (puriss. p.a., Sigma-Aldrich) and palladium(II) chloride (99.999%, Sigma-Aldrich) were mixed with hydrochloric acid (37%, AnalaR NORMAPUR) to prepare the sensitisation and activation solutions, respectively. The plating solution was prepared using tetraamminepalladium(II) chloride monohydrate (99.99% metals basis, Sigma-Aldrich), EDTA (IDRANAL®III, Riedel-deHaen), ammonium hydroxide (28% in H_2O, Sigma-Aldrich) and hydrazine hydrate (Sigma-Aldrich).

Fabrication of Asymmetric Al_2O_3 Hollow Fibres

Asymmetric Al_2O_3 hollow fibres were fabricated using the phase inversion/sintering method (Kingsbury and Li, 2009). Arlacel P135 was dissolved in DMSO prior to the addition of aluminium oxide. The mixture was rolled/milled for 48 h. After this, the polymer was added to the mixture and the suspension was rolled/milled for a further 48 h. The suspension was then transferred to a gas tight reservoir and degassed under vacuum. After degassing, the spinning suspension was extruded through a tube-in-orifice spinneret (outer diameter 3 mm, inner diameter 1.2 mm) into the external coagulation bath with water at different air gaps (distance between the fibre precursor and the external coagulant bath). Extrusion rates of 7 and 5 $mL{\cdot}min^{-1}$ were adopted for the ceramic suspension and bore fluid, respectively.

Fibre precursors were kept in water for 12 h in order to remove the excess of solvent and to allow complete phase inversion. The fibre precursors were then cut to the desired length, put in a straight position, dried for 48 h under atmospheric conditions and finally sintered in a tubular furnace (Elite, Model

TSH 17/75/450). In the sintering process, the temperature was increased up to 600 °C at a rate of 2 °C min^{-1} followed by a dwell of 2 h. In a second stage, the temperature was increased up to 1300 or 1400 °C (target temperature) at a rate of 5 °C min^{-1} followed by a dwell of 4 h. After that, the temperature was decreased to 25 °C at a rate of 3 °C min^{-1}. Figure 1 presents a flowchart with the steps carried out for the asymmetric hollow fibre preparation.

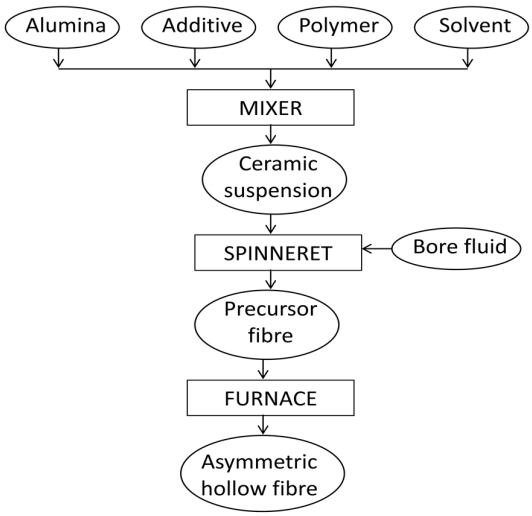

Figure 1: Flowchart of the spinning process.

The different parameters applied in the fabrication of each fibre are described in Table 1. The fibre HF1-1400 was prepared using water as the internal coagulant. Water is responsible for the coagulation of the ceramic suspension and, consequently, for the formation of micro-voids across the fibre. Using water as internal and external coagulants (Fibre HF1-1400) an air gap is necessary in order to allow the formation of the sponge-like layer in the outer surface of the fibre; otherwise the micro-voids would be formed in the inner and outer surfaces of the fibre. The fibre HF1-1400 was sintered at 1400 °C. No air gap was used during the fabrication of the fibres HF2-1300, HF3-1300 and HF3-1400 since solvent or a mixture of solvent with water were used as the internal coagulants. In these fibres (HF2-1300, HF3-1300 and HF3-1400) the micro-void formation was from the outer to the inner surface of the fibre due to the action of water that was used as external coagulant. The use of solvent as internal coagulant prevents precipitation or increased local viscosity at the inner surface before the solvent is finally exhausted. The fibre HF2-1300 was sintered at 1300 °C. For the fibres HF3-1300 and HF3-1400 the applied sintering temperatures were 1300 and 1400 °C, respectively.

Table 1: Fabrication parameters of the fibres.

Fibre	Internal Coagulant	Air Gap (cm)	Sintering Temperature (°C)
HF1-1400	Water	3	1400
HF2-1300	Solvent	0	1300
HF3-1300	Solvent+Water	0	1300
HF3-1400	Solvent+Water	0	1400

Characterisations of Asymmetric Al_2O_3 Hollow Fibres

The microstructure of each produced hollow fibre was characterized by scanning electron microscopy (EVO MA 10, Carl Zeiss). The surface micrograph and the average roughness of the hollow fibres were verified using atomic force microscopy (AFM, Shimadzu, SPM-9600).

The bending strength (σ_F) of the hollow fibres was determined by the bending test using an Instron Model 4466 provided with a load cell for 1 kN and was calculated using Equation (1) (Cernica, 1977; Othman *et al.*, 2010).

$$\sigma_F = \frac{8FLD_o}{\left(D_o^4 - D_i^4\right)} \tag{1}$$

where F is the measured load in which the fracture occurred (N), L is the length of the sample (m), and D_o and D_i are the outer and the inner diameters of the sample, respectively.

Nitrogen (N_2) and water (H_2O) flow rate measurements were carried out at different transmembrane pressures and at room temperature (approximately 25 °C) in order to investigate the permeability of the prepared hollow fibres. For these flow rate measurements, the hollow fibre with one-end sealed was glued with epoxy-resin (Araldite®) on a stainless steel holder that was connected to the permeation apparatus (Figure 2(a)). For nitrogen flow rate tests, the gas feed pressure was adjusted using a pressure regulator (OMEGA, PRG101-120) and monitored using a pressure gauge with a resolution of 0.1 psi (OMEGA, DPG1000B-10G). The gas was fed to the shell side of the fibre and collected from the lumen side. The N_2 flow rate was measured at several transmembrane pressures using gas rotameters. The water flow rate was measured in a cross-flow configuration, as shown in Figure. 2(b). The mass flow rate of the permeated water was measured at several transmembrane pressures and the flux was calculated by applying Equation (2):

$$J = \frac{m}{A\,t} \quad (2)$$

where J is the flux (kg m^{-2} s^{-1}), m is the permeated mass (kg), A is the effective surface area of the fibre (m^2) and t is the time of the permeate collection (s).

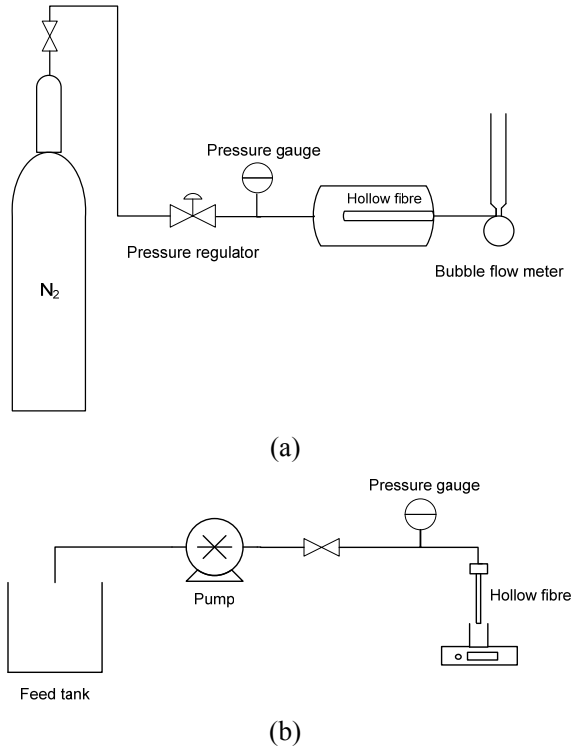

Figure 2: Schematic diagram of the nitrogen (a) and water (b) permeation apparatus.

Electroless Plating Procedure for Palladium Coating on Asymmetric Hollow Fibre Substrates

Palladium membranes were coated onto the outer surface of asymmetric hollow fibre substrates using the electroless plating procedure (Paglieri and Way, 2002; Mardilovich *et al.*, 1998). The coating was carried out on a length of 7 cm of the fibre and the ends of the fibre were coated with a gas-tight glaze.

According to the electroless plating procedure, the substrates were first activated with Pd nuclei via sensitisation in an acidic $SnCl_2$ solution followed by activation in an acidic $PdCl_2$ solution. The sensitisation/activation process was carried out by immersing the glazed hollow fibre substrates sequentially in five chemical baths: acidic $SnCl_2$ solution for 5 min; deionised water for 5 min, acidic $PdCl_2$ solution for 5 min; 0.01 M HCl solution for 2 min; and finally deionised water for 3 min. All chemical baths were homogenised with air bubbles. The sensitisation/activation process was repeated for 8 cycles. The composition of each bath is presented in Table 2.

Table 2: Sensitisation, activation and plating bath compositions.

Step	Compound	Concentration
Sensitisation	$SnCl_2$	1 g L^{-1}
	HCl (37%)	1 mL L^{-1}
Activation	$PdCl_2$	0.1 g L^{-1}
	HCl (37%)	1 mL L^{-1}
Rinsing	HCl	0.01M
Electroless Plating	$Pd(NH_3)4Cl_2$-H2O	4 g L^{-1}
	Na_2EDTA-$2H_2O$	40.1 g L^{-1}
	NH_3-H_2O (28%)	198 mL L^{-1}
	N_2H_4 (1M)	5.6 mL L^{-1}

After the sensitisation/activation step, the substrates were immersed in a Pd electroless plating solution at 60 °C for 60 min in order to deposit metallic Pd layers onto the activated surface. The plating solution was prepared according to the composition presented in Table 2 using a volume of 3.5 mL per cm^2 of substrate surface area, as suggested by Mardilovich *et al.* (1998).

The thicknesses and the roughness of the membranes were measured using SEM and AFM images, respectively.

Hydrogen Permeation Through Pd/Al_2O_3 Composite Hollow Fibre Membranes

Hydrogen (H_2) permeation measurements were performed using the experimental apparatus shown in Figure 3. The Pd/Al_2O_3 composite hollow fibre membrane with one-end sealed was glued to a stainless steel holder using epoxy-resin (Araldite®) and then introduced into a stainless steel tube. This tube was placed centred in a tubular furnace (CARBOLITE, MTF 10/25/130) and connected to inlet and outlet streams. The permeate flow rate was monitored by a bubble flow meter and the feed pressure was adjusted using a pressure regulator (OMEGA, PRG101-120) and monitored by a pressure gauge with a resolution of 0.1 psi (OMEGA, DPG1000B-10G).

Hydrogen permeation flow rates were measured at different temperatures (450-300 °C) and transmembrane pressures. Temperatures higher than 300 °C were chosen in order to prevent hydrogen embrittlement in the palladium membrane. At temperatures below 300 °C, Pd undergoes a phase transition which alters its microstructure, causing it to become brittle and subsequently fracture. Moreover, palladium membranes can be used in membrane reactors for the hydrogen production by steam methane reforming, which is carried out at temperatures higher than 300 °C.

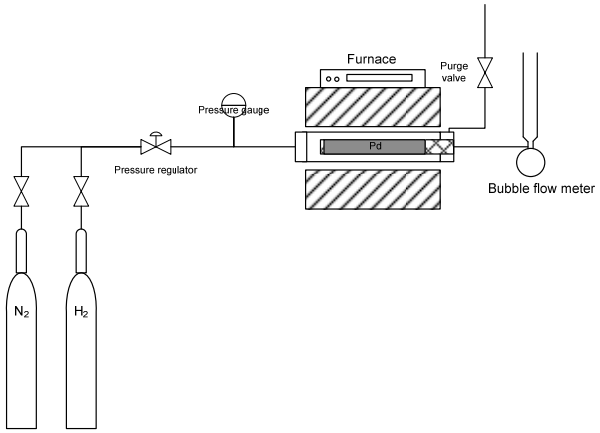

Figure 3: Schematic representation of the apparatus used for hydrogen permeation tests.

The system temperature was increased up to 450 °C at a heating rate of 3 °C min^{-1} under nitrogen purge at atmospheric pressure. The decrease of the temperature was carried out at a rate of 3 °C min^{-1} under nitrogen purge and membrane integrity was evaluated at each temperature for pressures up to 300 kPa. Hydrogen permeation tests were conducted exclusively on membranes which were gas-tight to nitrogen.

RESULTS AND DISCUSSION

Comparison of Asymmetric Hollow Fibres Prepared Under Different Conditions

Figure 4 shows the SEM images of each produced fibre. The obtained hollow fibres presented the desired asymmetric morphological structure, with an outer sponge-like layer and inner micro-channels covering a large extension of the fibre. The inner micro-channels will ensure greater permeabilities through the fibre. The outer sponge like layer is denser than the inner micro-channels and will provide the required mechanical strength for the hollow fibre.

Depending on the applied sintering temperature and the internal coagulant used, the obtained hollow fibres presented different morphological aspects. When water is used as internal coagulant an air gap is necessary to form the external sponge-like layer due to the contact of the outer surface of the fibre with air that increases the viscosity at this surface, as shown in Figure 4(c1). Then the fibre is immersed in the coagulation bath containing water, but the growth of the finger-like voids from the outer surface of the fibre is inhibited due to the previous increase in the viscosity. The inner surface of the fibre is in contact with water since the suspension is extruded and hence phase inversion and the formation of fingers are initiated there. Figures 4(a1) and 4(b1) show that the micro-channels of the hollow fibre HF1-1400 were blocked in the inner layer of the fibre. Application of water as the internal coagulant can be responsible for a ceramic precipitation that blocked the formed micro-channels. This blockage will decrease the fibre permeability, besides making difficult the application of this fibre as a support for catalyst depositions, for instance. In fact, for this fibre (HF1-1400), there are two sponge-like layers, one inside and the other outside the fibre. Figure 4(c1) shows that the filaments were formed irregularly and not along the fibre. Moreover, the finger-like layer is dense and covers approximately 20% of the fibre extension.

When solvent is used as internal coagulant the outer surface of the fibre is directly immersed in the coagulation bath containing water (zero air gap) and an instantaneous precipitation occurs from the outer surface. The use of solvent as internal coagulant prevents precipitation or increased local viscosity at the inner surface before the solvent is finally exhausted. According to Figures 4(a2) and 4(b2), the fibre HF2-1300 has a structure of micro-channels that were opened in the inner layer of the fibre since solvent was used as internal coagulant instead of pure water, and the ceramic precipitation was minimised. Comparing Figures 4(c2) and 4(c1), it is possible to see that the micro-channels formed in the fibre HF2-1300 are thinner and more regular than those formed in the fibre HF1-1400 due to the action of the solvent as internal coagulant. However, the number of micro-channels formed in the fibre HF2-1300 was smaller than in the other fibres. When using solvent as internal coagulant, the filaments are formed from the outer to the inner surface of the fibre due to the presence of water in the external bath. Thus, application of pure solvent as internal coagulant did not ensure the formation of numerous micro-voids across the fibre.

Figures 4(a3) and 4(a4) show that the application of different sintering temperatures did not affect the morphology of the fibre, as also observed by Garcia-Garcia *et al.* (2011). Comparing Figures 4(c3) and 4(c4) with Figures 4(c1) and 4(c2), it is possible to see that the micro-channels of the fibres HF3-1300 and HF3-1400 are more numerous and longer than those of the fibres HF1-1400 and HF2-1300. Moreover, the sponge-like layers of the fibres HF3-1300 and HF3-1400 are thinner than the sponge-like layers of the fibres HF1-1400 and HF2-1300. However, the

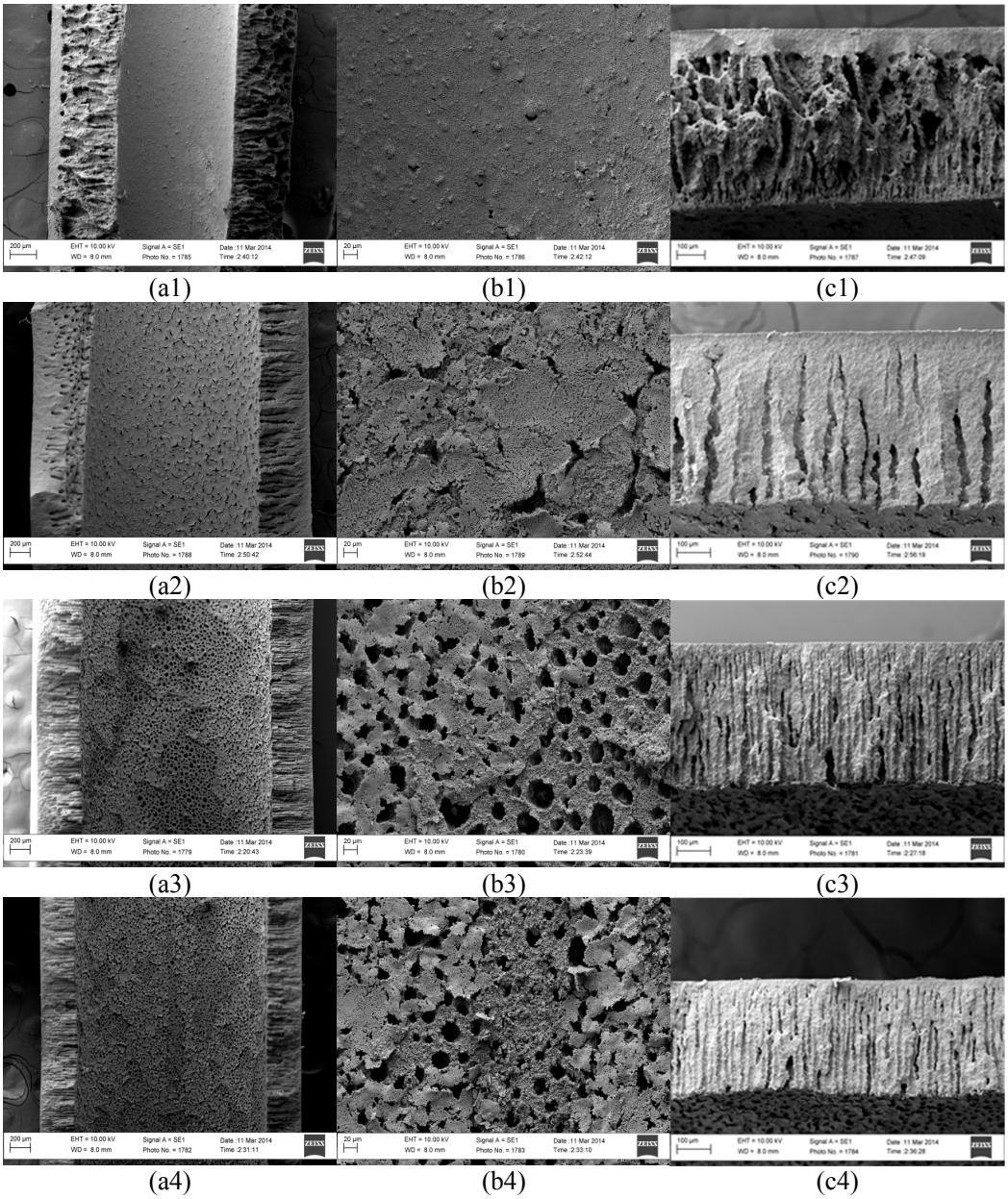

Figure 4: (a) Cross section, (b) inner surface and (c) fibre wall SEM images of the hollow fibres (1) HF1-1400, (2) HF2-1300, (3) HF3-1300, (4) HF3-1400.

micro-channels of the fibres HF3-1300 and HF3-1400 were also partially blocked, as shown in Figures 4(b3) and 4(b4). Then, the morphological analysis of the produced fibres showed that longer, organized and numerous micro-channels are obtained when using a mixture of solvent with water as internal coagulant, and, since no pure water was used as internal coagulant, the micro-channels remained partially open in the inner surface of the fibre. Figures 4(c3) and 4(c4) show that when a mixture of solvent with water is used as internal coagulant some fingers are formed from the inner surface and thus, more fingers are obtained.

Figure 5 shows AFM images of the outer surface of the prepared hollow fibre membranes, which are presented in a 10×10 μm scanning area. The fibre HF3-1400 was not analysed since the structure of the fibres HF3-1300 and HF3-1400 were quite similar (Figures 4(a3) and 4(a4)). According to Figure 5, all hollow fibres presented a rough surface, which consist of peaks and valleys. The hollow fibre HF1-1400 (Figure 5(a)) present less sharp peaks, probably due to the higher extension of the sponge-like layer (Figure 4(c1)).

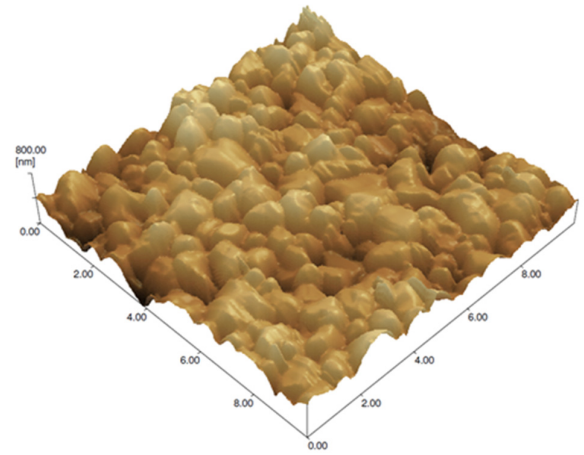

(a)

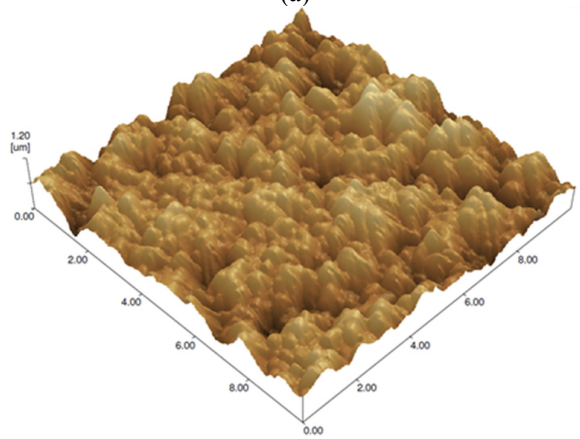

(b)

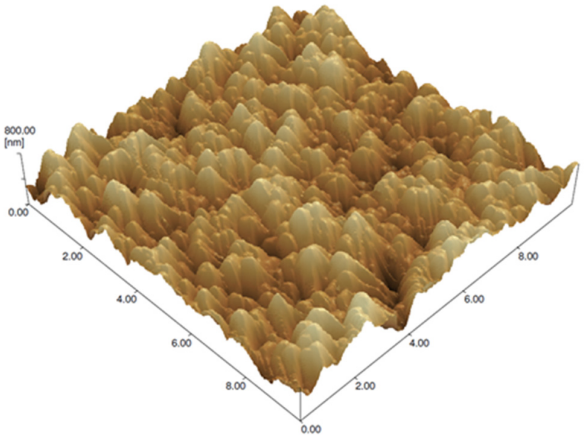

(c)

Figure 5: AFM images of the hollow-fibres (a) HF1-1400, (b) HF2-1300 and (c) HF3-1300.

According to the AFM images, mean and square roughness (Ra and Rq, respectively) were calculated for each hollow fibre (Table 3). The fibre HF1-1400 presented the smallest surface roughness, followed by the fibres HF3-1300 and HF2-1300. Thus, the use of water as internal coagulant probably decreased the roughness of the outer surface of the fibre due to the formation of the micro-voids from the inner to the outer surface of the fibre. Moreover, as also observed by Wei *et al.* (2008), the increase in the sintering temperature (fibres HF1-1400 and HF2-1300) could have decreased the roughness of the outer surface of the fibre due to the higher densification of the sponge-like layer at higher temperatures.

Table 3: Mean and square roughness (Ra and Rq, respectively) of each hollow fiber for a scan area of 10×10 µm.

Sample	Ra (nm)	Rq (nm)
HF1-1400	87.56	110.56
HF2-1300	125.72	158.65
HF3-1300	100.86	124.71

The mechanical strengths of the fibres HF1-1400, HF2-1300, HF3-1300 and HF3-1400 were equal to 70.3, 55.5, 41.2 and 74.5 MPa, respectively. Although all fibres presented high porosity, they did not present a high fragility. In fact, the fragility of the fibres increased with the increase of the micro-channel region. Moreover, related to the densification of the sponge-like layer, the decrease in the sintering temperature decreased the mechanical strength of the hollow fibre. Sun *et al.* (2006) produced asymmetric hollow fibres using different internal and external coagulant concentrations and obtained fibres with mechanical strengths varying from 36.3 to 122.6 MPa. However, the highest mechanical strength reported by Sun *et al*. (2006) (122.6 MPa) was attributed to a fibre without micro-channels.

Table 4 presents the measured water flow rate through the fibres according to the transmembrane pressure. The areas of the hollow fibres HF1-1400, HF2-1300, HF3-1300 and HF3-1400 used in these measurements were 7.10, 2.16, 4.95 and 4.32 cm^2, respectively. These data were used to calculate the water flux according to Equation (2).

Table 4: Measured water flow rate through the fibres according to the pressure.

Pressure (psi)	Water flow rate (L h^{-1})			
	HF1-1400	HF2-1300	HF3-1300	HF3-1400
4	0.023	0.058	0.780	0.193
6	0.040	0.087	1.236	0.314
8	0.054	0.118	1.812	0.460
10	0.072	0.144	2.208	0.596
12	0.093	0.167	2.610	0.753
14	0.111	0.194	3.024	0.899
16	0.126	0.218	3.474	1.035

Figure 6 shows nitrogen permeance and water flux through the fibres. The gas flow through the fibre HF3-1300 was not measured since it was higher than the maximum value measured by the rotameter (10 L min^{-1}) even at lower pressures.

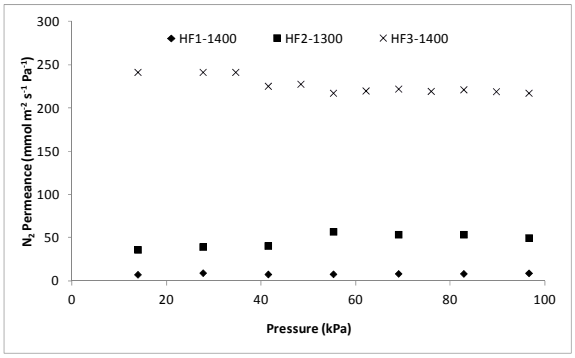

(a)

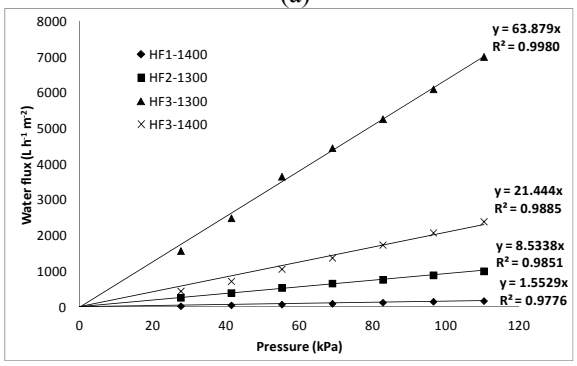

(b)

Figure 6: (a) Nitrogen permeance and (b) water flux through the hollow fibres HF1-1400, HF2-1300, HF3-1300 and HF3-1400.

The fibre HF3-1400, which has more filaments, presented the highest gas permeability (Figure 6a). It is important to consider that this fibre presented a relative high mechanical strength, due to the higher applied sintering temperature. The lowest N_2 permeability was observed for the fibre HF1-1400, probably due to the blockage of the micro-channels in the inner layer. The values of N_2 permeation through the fibre HF1-1400 are in agreement with values reported by Hatim *et al.* (2011) for a similar asymmetric hollow fibre.

Figure 6b shows the water flux through the proposed hollow fibres. All fluxes presented a linear behaviour with the pressure. The greater water flow was verified through the fibre HF3-1300, probably because of the greater length and the number of micro-channels. Comparing the water flow through the fibres HF3-1300 and HF3-1400, it is possible to verify that the increase in the sintering temperature decreased the permeability of the fibre by approximately 2%, due to the densification of the sponge-like layer. Similarly for gas permeation, the fibre HF3-1400 presented higher water permeability than the fibres HF2-1300 and HF1-1400. Wu *et al.* (2013) evaluated the water flow through an asymmetric hollow fibre with similar structure to HF1-1400. Values of water flow through the fibre HF1-1400 are in agreement with the values given by Wu *et al*. (2013).

Effect of the Substrate on Hydrogen Permeation Through Composite Palladium Membranes

The hydrogen flow rate was measured through composite Pd/Al_2O_3 membranes using as substrate the asymmetric hollow fibres HF1-1400 and HF3-1400. According to the SEM images (Figure 7), the coated Pd membranes presented thicknesses of 1.8 and 1.4 μm using the hollow fibres HF1-1400 and HF3-1400 as supports, respectively. The Pd coating was carried out in separated baths, so that this difference in the thickness could be expected even using identical electroless plating conditions.

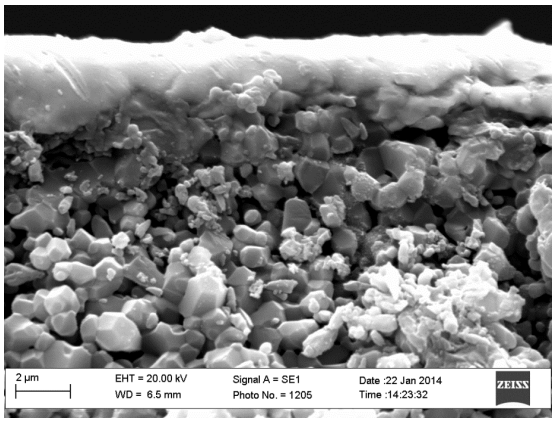

(a)

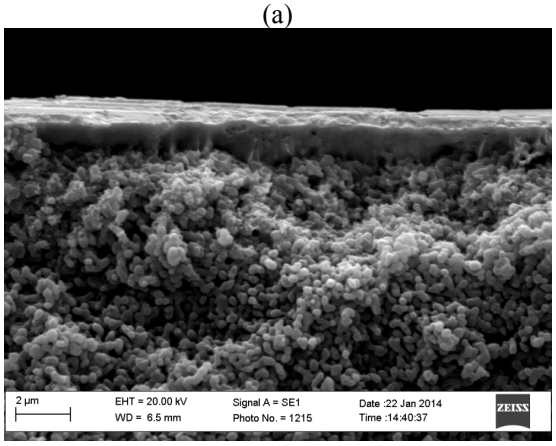

(b)

Figure 7: Cross-section SEM images of the asymmetric Pd/Al_2O_3 composite membranes supported on the hollow fibres HF1-1400 (a) and HF3-1400 (b).

Figure 8 presents the AFM image of the fibre HF1-1400 after the coating with Pd. Comparing Figures 5(a) and 8, it is possible to see that the outer surface of the membrane becomes smoother after the Pd deposition. Values of mean and square roughness for the Pd/HF1-1400 composite membrane were 67.21 and 83.13 nm, respectively, which represent values 1.3 times greater than for the substrate used.

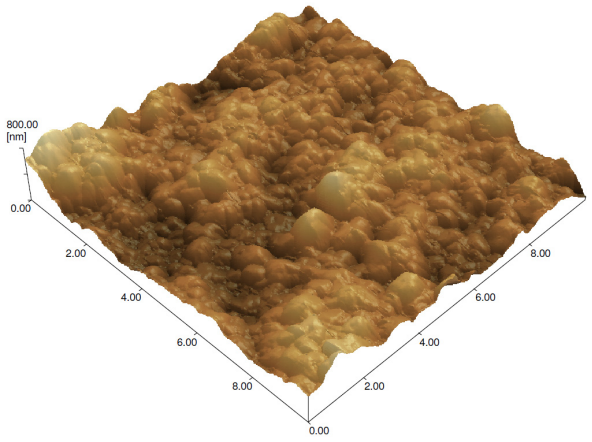

Figure 8: AFM image of the asymmetric Pd/Al_2O_3 composite membranes supported on the hollow fibre HF1-1400.

Figure 9 presents the H_2 permeation through the composite membranes prepared using HF1-1400 and HF3-1400 as substrates. The linear adjustment of H_2 flux with pressure was better than the adjustment according to Sievert's law (n=0.5), since the surface adsorption/desorption becomes the controlling step instead of bulk diffusion (Yun and Oyama, 2011).

Hydrogen flux increased with increases in the temperature and in the transmembrane pressure. Hydrogen permeances through the composite membrane prepared using the hollow fibre HF3-1400 as substrate was approximately 60 times greater than using the hollow fibre HF1-1400. The composite membrane Pd/ HF1-1400 reached a H_2 flux similar to the highest ones reported in the literature (0.40 mol m^{-2} s^{-1} at 100 kPa and 450 °C for composite membranes using ceramic supports (Yun *et al.*, 2011; Zhao *et al.*, 1998). However, Yun *et al.* (2011) and Zhao *et al.* (1998) applied a modified electroless procedure in order to deposit thinner and selective Pd membranes on the ceramic supports.

Then, application of Al_2O_3/Pd asymmetric hollow fibre composite membranes presents advantages for hydrogen permeation of higher ratios of area and volume and less resistance to mass transfer.

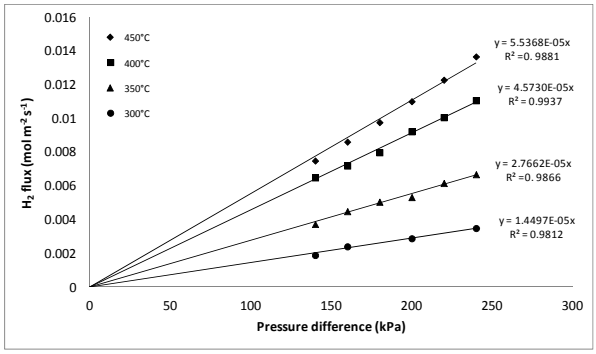

(a)

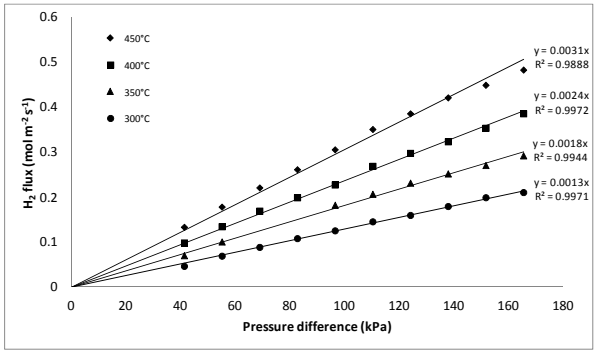

(b)

Figure 9: Hydrogen flux through asymmetric Pd/Al_2O_3 composite hollow fibre membranes supported on HF1-1400 (a) and HF3-1400 (b).

CONCLUSION

The proposed hollow fibres presented the required properties: high mechanical strength, smooth outer surface, presence of micro-channels in a large extension of the fibre, high porosity, and high nitrogen and water permeabilities. The decrease in the sintering temperature, from 1400 to 1300 °C, increased the permeabilities through the fibre. However, the decrease in the sintering temperature decreased the mechanical strength of the hollow fibre.

Moreover, the choice of the appropriate internal coagulant, responsible for the formation of the microchannels, is important to have a more permeable hollow fibre. Characterisation results showed that the application of a mixture of water and solvent as internal coagulant for the fabrication of hollow fibres ensured the formation of numerous and long microchannels that, consequently, resulted in high permeabilities through these fibres.

Hydrogen permeation measurements through composite Pd/Al_2O_3 membranes showed that the support employed has a great influence on the result obtained.

ACKNOWLEDGMENTS

The authors acknowledge Professor Kang Li for supporting hollow fibre preparations and the research funding provided by CNPq (Grant number: 407133/2013-5), CAPES and FAPEMIG (Grant numbers: TEC-PPM-00752-15 and TEC-APQ-01750-15).

REFERENCES

Cernica, J. N., Strength of Materials. 2nd Edition Ed., Holt Rinehart & Winston, New York (1977).

de Jong, J., Benes, N. E., Koops, G. H., Wessling, M., Towards single step production of multi-layer inorganic hollow fibers. Journal of Membrane Science, 239, pp. 265-269 (2004).

Dittmeyer, R., Hollein, V., Daub, K., Membrane reactors for hydrogenation and dehydrogenation processes based on supported palladium. J. Mol. Catal. A-Chem., 173, pp. 135-184 (2001).

Falbo, F., Tasselli, F., Brunetti, A., Drioli, E., Barbieri, G., Polyimide hollow fiber membranes for CO_2 separation from wet gas mixtures. Braz. J. Chem. Eng., 31, pp. 1023-1034 (2014).

Garcia-Garcia, F. R., Kingsbury, B. F. K., Rahman, M. A., Li, K., Asymmetric ceramic hollow fibres applied in heterogeneous catalytic gas phase reactions. Catalysis Today, 193, pp. 20-30 (2012).

Garcia-Garcia, F. R., Rahman, M. A., Kingsbury, B. F. K., Li, K., Asymmetric ceramic hollow fibres: New micro-supports for gas-phase catalytic reactions. Applied Catalysis A-General, 393, pp. 71-77 (2011).

Hatim, M. D. I., Tan, X. Y., Wu, Z. T., Li, K., Pd/Al_2O_3 composite hollow fibre membranes: Effect of substrate resistances on H-2 permeation properties. Chemical Engineering Science, 66, pp. 1150-1158 (2011).

Kingsbury, B. F. K., Li, K., A morphological study of ceramic hollow fibre membranes. Journal of Membrane Science, 328, pp. 134-140 (2009).

Lee, M., Wu, Z. T., Wang, R., Li, K., Micro-structured alumina hollow fibre membranes - Potential applications in wastewater treatment. Journal of Membrane Science, 461, pp. 39-48 (2014).

Li, K., Tan, X. Y., Liu, Y. T., Single-step fabrication of ceramic hollow fibers for oxygen permeation. Journal of Membrane Science, 272, pp. 1-5 (2006).

Liu, S. M., Li, K., Hughes, R., Preparation of porous aluminium oxide (Al_2O_3) hollow fibre membranes by a combined phase-inversion and sintering method. Ceramics International, 29, pp. 875-881 (2003).

Machado, P. S. T., Habert, A. C., Borges, C. P., Membrane formation mechanism based on precipitation kinetics and membrane morphology: Flat and hollow fiber polysulfone membranes. Journal of Membrane Science, 155, pp. 171-183 (1999).

Mardilovich, P. P., She, Y., Ma, Y. H., Rei, M. H., Defect-free palladium membranes on porous stainless-steel support. AIChE Journal, 44, pp. 310-322 (1998).

Othman, M. H. D., Wu, Z. T., Droushiotis, N., Doraswami, U., Kelsall, G., Li, K., Single-step fabrication and characterisations of electrolyte/anode dual-layer hollow fibres for micro-tubular solid oxide fuel cells. Journal of Membrane Science, 351, pp. 196-204 (2010).

Paglieri, S. N., Way, J. D., Innovations in palladium membrane research. Separ Purif. Method, 31, pp. 1-169 (2002).

Sun, G. B., Hidajat, K., Kawi, S., Ultra thin Pd membrane on alpha-Al_2O_3 hollow fiber by electroless plating: High permeance and selectivity. Journal of Membrane Science, 284, pp. 110-119 (2006).

Tan, X. Y., Liu, S. M., Li, K., Preparation and characterization of inorganic hollow fiber membranes. Journal of Membrane Science, 188, pp. 87-95 (2001).

Wei, C. C., Chen, O. Y., Liu, Y., Li, K., Ceramic asymmetric hollow fibre membranes-One step fabrication process. Journal of Membrane Science, 320, pp. 191-197 (2008).

Wu, Z. T., Faiz, R., Li, T., Kingsbury, B. F. K., Li, K., A controlled sintering process for more permeable ceramic hollow fibre membranes. Journal of Membrane Science, 446, pp. 286-293 (2013).

Yun, S., Oyama, S. T., Correlations in palladium membranes for hydrogen separation: A review. Journal of Membrane Science, 375, pp. 28-45 (2011).

Yun, S., Ko, J. H., Oyama, S. T., Ultrathin palladium membranes prepared by a novel electric field assisted activation. Journal of Membrane Science, 369, pp. 482-489 (2011).

Zhao, H. B., Pflanz, K., Gu, J. H., Li, A. W., Stroh, N., Brunner, H., Xiong, G. X., Preparation of palladium composite membranes by modified electroless plating procedure. Journal of Membrane Science, 142, pp. 147-157 (1998).